Synthesis and Characterization of CoFe 2 O 4 Nanoparticles Dispersed in a Silica Matrix by a Sol–Gel Autocombustion Method

ARTICLE *in* CHEMISTRY OF MATERIALS · AUGUST 2006

Impact Factor: 8.35 · DOI: 10.1021/cm060650n

4 AUTHORS:

Carla Cannas
Università degli studi di Cagliari
97 PUBLICATIONS **1,667** CITATIONS
SEE PROFILE

Anna Musinu
Università degli studi di Cagliari
121 PUBLICATIONS **2,634** CITATIONS
SEE PROFILE

Davide Peddis
Italian National Research Council
64 PUBLICATIONS **790** CITATIONS
SEE PROFILE

Giorgio Piccaluga
Università degli studi di Cagliari
141 PUBLICATIONS **3,320** CITATIONS
SEE PROFILE

Synthesis and Characterization of $CoFe_2O_4$ Nanoparticles Dispersed in a Silica Matrix by a Sol−Gel Autocombustion Method

C. Cannas,* A. Musinu, D. Peddis, and G. Piccaluga

Dipartimento di Scienze Chimiche, Cittadella Universitaria di Monserrato, Bivio per Sestu, 09042 Monserrato-Cagliari, Italy

Received March 17, 2006. Revised Manuscript Received June 1, 2006

A very fast self-combustion reaction was applied for the first time to the synthesis of a series of magnetic $CoFe_2O_4-SiO_2$ nanocomposites in a wide range of compositions (from 5 to 50 wt % $CoFe_2O_4$). Combining a gelation method that adopts metal nitrates, citric acid and tetraethoxysilane as precursors with controlled thermal treatments, a wide variety of samples with properties finely modulated were obtained. Particle formation and evolution of the structural and magnetic properties with the temperature were investigated by thermal analysis, X-ray diffraction, transmission electron microscopy, high-resolution transmission electron microscopy, nitrogen physisorption, IR, and magnetic susceptibility measurements. It was shown that the formation of metal ammonium carboxylate complexes takes place in all the gel precursors, contributing to the control of nucleation and growth of the nanoparticles. Spherical particles with narrow particle size distribution, uniformly dispersed in the matrix, are obtained in the diluted samples (N5, N10, N15), while nanoparticles with more irregular shapes form in samples with high $CoFe_2O_4$ content (N30, N50). Magnetic properties evolve with $CoFe_2O_4$ amounts and thermal treatments. The samples treated at 900 °C exhibit superparamagnetic behavior, with the expected dependence of the magnetic relaxation on particle size.

Introduction

Spinel ferrite magnetic nanoparticles have attracted great interest because of their unusual physical properties (for instance, superparamagnetism) and their practical applications in several fields (for instance, in high-density information storage, ferrofluid technology, and magnetically guided drug delivery).[1−6] Therefore, a great variety of methods have been experimented with for their preparation, such as chemical precipitation, sol−gel processing, microemulsion route, sonochemistry, hydrothermal processing, aerosol-vapor methods, and high-temperature decomposition of organic precursors.[2,4−6] Recently, a sol−gel autocombustion method has been proposed for ferrite synthesis,[7−10] and we have applied it to the preparation of cobalt ferrite, $CoFe_2O_4$.[11−13] In this method, precursor gels are prepared from aqueous solutions of metal nitrates and an organic complexant such as citric acid. The nitrate citrate gels, when heated in a hot furnace, burn in a self-propagating process, rapidly converting the precursor mixtures directly into products.

However, it is well-known that magnetic nanoparticles tend to agglomerate, not only because of their large surface energy, but also because of their strong magnetic interactions. Therefore, for both fundamental and applied investigations, magnetic properties are more profitably studied by preparing the samples in the form of nanocomposites, that is, by dispersing the magnetic particles in inert matrixes (amorphous SiO_2 is frequently used, but also polymers and resins are common).[14−19] Moving along these lines, we have already shown that the mentioned sol−gel autocombustion method can be adapted to synthesize cobalt ferrite−silica nanocomposites.[11,12] In these[11−13] and similar studies by other authors,[20,21] only the compositional range rich in ferrite has been considered.

* To whom correspondence should be addressed. Fax: +39 070 6754388. E-mail: ccannas@unica.it.

(1) Leisle-Pelecky, D. L.; Rieke, R. D. *Chem. Mater.* **1996**, *8*, 1770.
(2) Carpenter, E. E.; O'Connor, C. J. *J. Appl. Phys.* **1999**, *85*, 8, 5175.
(3) Pankhurst, Q. A.; Connolly, J.; Jones, S. K.; Dobson, J. *J. Phys. D: Appl. Phys.* **2003**, *36*, R167 and references therein.
(4) Tartaj, P.; Morales, M.; Venitemillas-Verdaguer, S.; Gonzales-Carreno, T.; Serna, C. J. *J. Phys. D: Appl. Phys.* **2003**, *36*, R182 and references therein.
(5) Vestal, C. R.; Zhang, Z. J. *Int. J. Nanotechnol.* **2004**, *1*, 240 and references therein.
(6) Vijaya Kumar, R.; Diamant, Y.; Gedanken, A. *Chem. Mater.* **2000**, *12*, 2301.
(7) Mishra, S. K.; Pathak, L. C.; Rao, V. *Mater. Lett.* **1997**, *32*, 137.
(8) Yue, Z.; Zhou, J.; Li, L.; Zhang, H.; Gui, Z. *J. Magn. Magn. Mater.* **2000**, *21*, 55.
(9) Yue, Z.; Zhou, J.; Wang, X.; Gui, Z.; Li, L. *J. Mater. Sci. Lett.* **2001**, *20*, 1327.
(10) Qi, X.; Zhou, J.; Yue, Z.; Gui, Z.; Li, L. *Ceram. Int.* **2003**, *29*, 347.
(11) Cannas, C.; Musinu, A.; Peddis, D.; Piccaluga, G. *J. Nanopart. Res.* **2004**, *6*, 223.
(12) Cannas, C.; Falqui, A.; Musinu, A.; Peddis, D.; Piccaluga, G. *J. Nanopart. Res.*, in press.
(13) Cannas, C.; Falqui, A.; Musinu, A.; Peddis, D.; Piccaluga, G. *J. Nanopart. Res.*, submitted for publication.
(14) Ennas, G.; Musinu, A.; Piccaluga, G.; Zedda, D.; Gatteschi, D.; Sangregorio, C.; Stanger, J. L.; Concas, G.; Spano, G. *Chem. Mater.* **1998**, *10*, 495.
(15) Cannas, C.; Gatteschi, D.; Musinu, A.; Piccaluga, G.; Sangregorio C. *J. Phys. Chem. B* **1998**, *102*, 40, 7721.
(16) Plocek, J.; Hutlòva, A.; Niznansky, D., Bursik, J.; Rehspringer, J. L.; Micka, Z. *J. Non-Cryst. Solids* **2003**, *315*, 70.
(17) Hutlova, A.; Niznansky, D.; Rehspringer, J. L.; Estournès, C.; Kurmoo, M. *Adv. Mater.* **2003**, *15*, 1623.
(18) Tejada, J.; Ziolo, R. F.; Zhang, X. X. *Chem. Mater.* **1996**, *8*, 1784.
(19) Del Barco, E.; Asenjo, J.; Zhang, X. X.; Pieczynsk, R.; Julià, A.; Tejada, J.; Ziolo, R. F.; Fiorani, D.; Testa, A. M. *Chem. Mater.* **2001**, 131487.
(20) Wu, K. H.; Chang, Y. C.; Wang, G. P. *J. Magn. Magn. Mater.* **2004**, *269*, 150.

10.1021/cm060650n CCC: $33.50
Published on Web 07/13/2006

Table 1. Preparation Conditions of the Starting Sol

sample	acronym	ICP [$CoFe_2O_4$] (wt %)	ICP [SiO_2] (wt %)	TEOS (mol)	Et(OH) (mol)	H_2O (mol)	citric acid (mol)	$Co(NO_3)_2$ (mol)	$Fe(NO_3)_3$ (mol)
$CoFe_2O_4/SiO_2$, 50 wt %	N50	49.5	50.5	0.0130	0.76	1.29	0.0100	0.00340	0.00680
$CoFe_2O_4/SiO_2$, 30 wt %	N30	29.0	71	0.0304	0.76	1.29	0.0100	0.00340	0.00680
$CoFe_2O_4/SiO_2$, 15 wt %	N15	16.0	84	0.0746	1.18	1.29	0.0100	0.00340	0.00680
$CoFe_2O_4/SiO_2$, 10 wt %	N10	10.5	89.5	0.0304	0.76	1.29	0.00262	0.000881	0.00179
$CoFe_2O_4/SiO_2$, 5 wt %	N5	4.7	95.3	0.0304	0.76	1.29	0.00125	0.000417	0.000836

In the past, iron oxide−silica-based nanocomposites have been prepared in our laboratories by the classical sol−gel method, in which the starting solution contained metal salts, water, ethanol, and tetraethyl orthosilicate (TEOS).[14,15,22] Following this route, the nanoparticles nucleate and grow inside a preformed silica network and their morphological and geometrical features are mainly affected by the properties of the host matrix (porosity, surface area); in these conditions the control of particle size and distribution is quite difficult. In the autocombustion method the formation of the nanoparticles is directly influenced also by the carboxylate−metal complexes that form during the gelation stage and which give rise to the metal oxides during the combustion. For this reason the control of the properties of the nanoparticles should be easier. Therefore, we tried to extend the complexation−autocombustion method to the preparation of ferrite−silica nanocomposites in a rather wide range of compositions, down to the dilute nanocomposites, that have never been prepared by this route. In the present paper we describe the preparation of $(CoFe_2O_4)_x(SiO_2)_{1-x}$ samples, with $x = 50$, 30, 15, 10, and 5 wt %, and a thorough characterization of the products by transmission electron microscopy (TEM), high-resolution TEM (HRTEM), X-ray diffraction (XRD), differential thermal analysis (DTA), thermogravimetry (TG), nitrogen physisorption, IR spectroscopy, and magnetic measuments.

Experimental Section

Five $(CoFe_2O_4)_x(SiO_2)_{1-x}$ nanocomposites, with $x = 50$, 30, 15 10, and 5 wt %, were synthesized, adjusting a procedure described elsewhere[11−13] in which a traditional sol−gel technique (hydrolysis and condensation of alkoxide precursors) is combined with the sol−gel autocombustion. In the following, the samples will be indicated by the acronyms N50, N30, N15, N10, and N5, respectively (Table 1).

Tetraethoxysilane (TEOS, Aldrich, 98%) was used as a precursor for the SiO_2, whereas metal nitrates ($Fe(NO_3)_3 \cdot 9H_2O$, Aldrich, 98%, and $Co(NO_3)_2 \cdot 6H_2O$, Aldrich, 98%) and citric acid were used as precursors for the $CoFe_2O_4$ nanoparticles. The iron and cobalt nitrates were dissolved in water with a 2:1 molar ratio, and citric acid (CA, Aldrich, 99.5%) was added to the solution. The molar ratio of metals (Co(II) + Fe(III)) to CA was fixed at 1:1. The corresponding citrate-to-nitrate ratio was 0.37 in all the gels. The resulting clear purple solution had a spontaneous pH value <1. Liquor ammonia (Carlo Erba, 25%) was added dropwise to adjust the pH value to 2. A suitable amount of TEOS in ethanol was then added to the aqueous solution, and a few drops of ammonia were also added to bring the pH back to the value of 2. All the mixtures appeared clear and did not exhibit any phase separation.

After vigorous stirring for 30 min, the sols were poured into Teflon beakers and allowed to gel in static air at 40 °C in an oven for 24 h.

The thermogravimetric analysis of the gels, described below, showed that the decomposition of the precursors is complete at temperatures between 200 and 230 °C. On this basis, the gels were submitted to thermal treatment at 300 °C in a preheated oven. After elimination of large amounts of gases, the gels burned through a self-propagating process, producing directly $CoFe_2O_4/SiO_2$ nanocomposites (as-prepared samples) in powder form. The temperature was raised to 900 °C with steps of 100 °C, and the samples were kept at each temperature for 1 h.

The pH and preparation conditions reported in Table 1 were selected after a long series of trial experiments, in which the effect of each of several parameters was explored. The preparation of composites is, in fact, more difficult than that of pure phases.

To obtain composites in which the active phase is well dispersed in the silica matrix, the gelation time of the silica precursor has to be similar to that of the metal citrate complex. However, at the pH conditions usually reported in the literature for the preparation of pure ferrite (pH 7), TEOS hardly polymerizes and is mostly eliminated during the self-combustion reaction, leading to pure metal oxides. Nanocomposites with a high load of active phase were successfully obtained at pH 4 and a gelation temperature of 40 °C.[11] The pH value of 2 and gelation temperature of 40 °C were found to be the best compromise to prepare homogeneous sols in a more extended range of compositions. In such conditions it was possible to obtain the desired nanocomposites, with good nanoparticle dispersion and size distribution.

The addition of ethanol as a mutual solvent can lead to phase separation because of the decreased solubility of metal citrate complexes;[23] therefore, also the amount of ethanol is a critical parameter. Besides, to get homogeneous sols, when the amount of TEOS is increased, the amount of ethanol has to be increased in going from N50 to N15. However, a further increase of TEOS and ethanol for the diluted (N10 and N5) samples would lead to great differences in the sol surface:volume ratio and therefore to quite different gelation times.[22] For this reason, in the diluted samples the amount of salts was decreased instead of the TEOS and ethanol amounts being increased.

The composition and the iron-to-cobalt ratio in all composites were checked by inductively coupled plasma analysis; the results confirmed the nominal composition with an instrumental error of about 2% (Table 1), including the iron-to-cobalt molar ratios of 2.

The structural evolution of the samples was monitored by XRD, using a Siemens D500 diffractometer with $\theta-2\theta$ Bragg Brentano geometry and a Mo Kα wavelength. Cobalt ferrite nanoparticles were observed in electron micrographs obtained by a transmission electron microscope (JEOL 200CX) operating at 200 kV. Finely ground samples were dispersed in octane and subjected to an ultrasonic bath. The suspensions were then dropped on carbon-coated copper grids for the observations. The particle size was obtained by measuring in different parts of the grid the average diameter D_i of a number of particles close to 100 in the diluted samples and to 500 in the most concentrated ones.

(21) Wu, K. H.; Huang, W. C.; Yang, C. C.; Hsu, J. S. *Mater. Res. Bull.* **2005**, *40*, 239.
(22) Cannas, C.; Concas, G.; Gatteschi, D.; Musinu, A.; Piccaluga, G.; Sangregorio, C. *J. Mater. Chem.* **2002**, *12* (10), 3141.
(23) Hao, X.; Wei, Y.; Zhang, S. *Transition Met. Chem.* **2001**, *26*, 384.

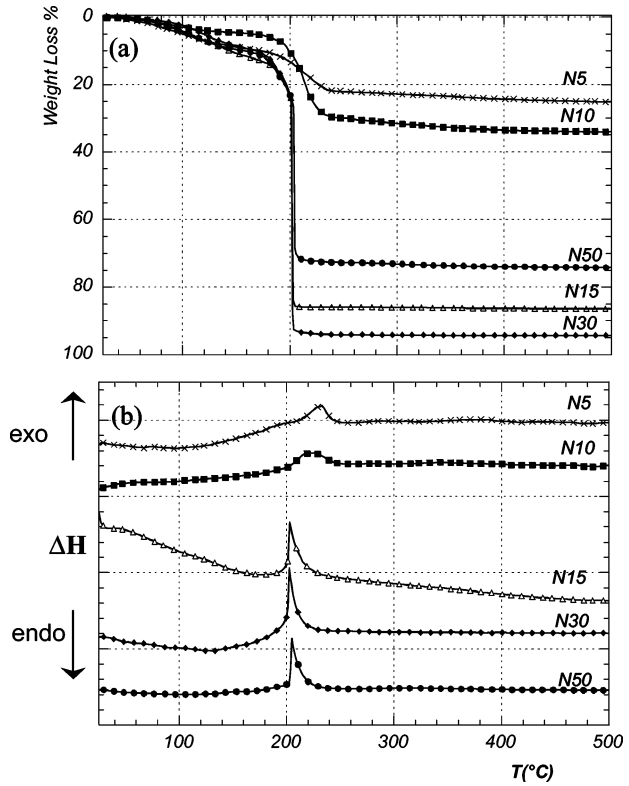

Figure 1. TG (a) and DTA (b) plots of the N50, N30, N15, N10, and N5 fresh gels.

HRTEM images were obtained by a JEM 2010 UHR equipped with a Gatan imaging filter (GIF) and a 794 slow scan CCD camera.

TG and simultaneous DTA were carried out on a Mettler-Toledo TGA/SDTA 851 in the 25−1000 °C range, with a heating rate of 10 °C/min under 50 mL/min oxygen flow.

IR spectra were collected in the middle region from 400 to 2000 cm^{-1} using a Bruker Equinox 55 spectrophotomer on KBr pellets.

Textural analysis was carried out by a Sorptomatic 1990 system (Fisons Instruments, Rodano (Mi), Italy) by determining the nitrogen adsorption/desorption isotherms at 77 K. Before analysis, the samples were heated under vacuum to 220 °C, with a rate of 1 °C/min, and kept at 220 °C for 12 h (as-prepared samples) and at 400 °C for 10 h (calcined samples). The specific surfaces were assessed by the BET method[24] in the case of mesoporous samples and by the Dubinin method[25] in the case of highly microporous samples.

Measurements of static magnetic moment were performed by a Quantum Design SQUID magnetometer, equipped with a superconducting magnet able to produce fields of up to 5 T. The samples were immobilized in an epoxy resin to prevent any nanoparticle movement. The samples were cooled in zero magnetic field, and then the zero-field-cooled (ZFC) susceptibility was measured by increasing the temperature in an applied field of 50 Oe, while the field-cooled (FC) susceptibility was recorded by cooling the samples in the same field.

Results

Gel Precursors. Figure 1 shows the TG and DTA profiles of the fresh gels with different metal contents. All the gels display weight losses from 7% to 17% in the 50−190 °C temperature range, related to the elimination of ethanol and water, and a drastic weight loss at 200−230 °C, accompanied by an exothermic asymmetric peak in the DTA curves, due to the self-combustion mechanism.[7−10,26−28] The total weight losses depend not only on the metal salt amounts, but also on the different amounts of ethanol, water, and citric acid entrapped inside the gel, and even on the different quantities of ammonia used to adjust the pH. The weight loss at about 200 °C is mainly affected by the metal content: it decreases with decreasing metal content from a value of about 60−80% in N15, N30, and N50 to 10−20% in N5 and N10, while the sharp asymmetric exothermic peak centered at about 202−203 °C shifts to 223−230 °C and becomes broader and its intensity decreases considerably. This effect is due to the high content of silica that hampers the self-propagating combustion process. No other important transformation can be evidenced in the TG−DTA curves at temperatures beyond 230 °C, indicating that at this temperature the precursors are completely decomposed.

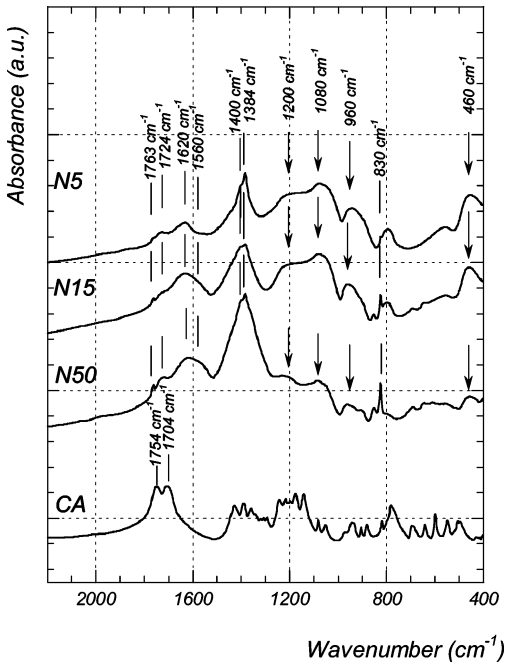

Figure 2. IR spectra of the N50, N15, and N5 fresh gels compared with citric acid (commercial product).

The mid-IR spectra of the N50, N15, and N5 gels are reported in Figure 2, together with the spectrum of pure CA. Important information is contained in the 1300−1950 cm^{-1} region, in which the signals of the vibrational modes of the carboxyl groups are observed. The spectrum of pure CA shows a doublet in the range 1650−1800 cm^{-1}, attributed to stretching vibration absorption bands of carboxylic groups, which can be ascribed to free carboxylic groups (1754 cm^{-1}) and carboxylic groups forming intramolecular hydrogen bonds (1704 cm^{-1}).[29] A small broad doublet shifted to higher values (1763 and 1724 cm^{-1}) is also visible in the spectra of the gel precursors. Its incomplete disappearance indicates

(24) Brunauer, S.; Emmet, P. H.; Teller, E. *J. Am. Chem. Soc.* **1938**, *60*, 309.
(25) Dubinin, M. M. *Q. Rev. Chem. Soc.* **1955**, *9*, 101.
(26) Chakraborty, A.; Devi, P. S.; Roy, S.; Maiti, H. S. *J. Mater. Res.* **1994**, *9*, 4, 986.
(27) Devi, P. S.; Maiti, H. S. *J. Mater. Res.* **1994**, *9*, 6, 1357.
(28) Shafer, S.; Sigmund, W.; Roy, S.; Aldinger, F. *J. Mater. Res.* **1997**, *12*, 10, 2518.
(29) Takahashi, R.; Sato, S.; Sodesawa, T.; Kawakita, M.; Ogura, K. *J. Phys. Chem. B* **2000**, *104*, 12184.

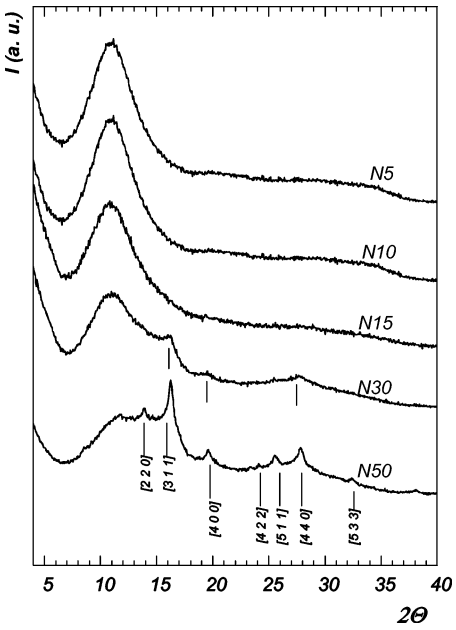

Figure 3. XRD patterns of the as-prepared samples.

that a small amount of free citric acid is still present in the precursor gels. In addition, four signals are present at about 1620, 1560, 1400, and 1384 cm^{-1}. The band at about 1620 cm^{-1}, together with the shoulder at about 1560 cm^{-1}, can be assigned to the asymmetric stretching O−C−O (ν_a) of the carboxylate anion, although the bending of water molecules can also contribute at around 1630 cm^{-1};[30] the intense signal at 1400 cm^{-1} is due to symmetric stretching of O−C−O groups and to N−H stretching of the NH_4^+ ions. These three bands are typical of a three-dimensional structure of a metal ammonium carboxylate gel,[31] confirming the formation of metal complexes in all the samples. The very sharp band at 1384 cm^{-1} is attributable to the stretching vibration of NO_3^- ions; another sharp band clearly visible at 830 cm^{-1} is also ascribable to the NO_3^- ions. The presence of these two signals indicates that NO_3^- exists as a free group in the structure of the citrate gel and provides an in situ oxidizing environment for the combustion of the citrate component.[32]

The typical bands of silica gel (highlighted with arrows in Figure 2) at about 1200, 1080, 960, and 460 cm^{-1} are also present; their intensity increases with decreasing metal content, confirming the expected formation of the silica network in higher amount in the diluted systems.[33] These observations undoubtedly indicate that the precursor gels are formed by a silica network embedded by metal ammonium carboxylate complexes.

As-Prepared Samples. The XRD results are reported in Figure 3. Only the amorphous pattern of the silica matrix is visible in the case of diluted samples (N15, N10, and N5). With the increase of the $CoFe_2O_4$ content, three broadened peaks appear (N30), and then new and sharper reflexes with increased intensity emerge (N50), indicating the presence of a nanocrystalline phase. The whole pattern can be ascribed to the $CoFe_2O_4$ spinel phase (PDF 22-1086); no shift is observed in the *d* spacings compared with the theoretical card, thus confirming the formation of a stoichiometric cobalt ferrite.

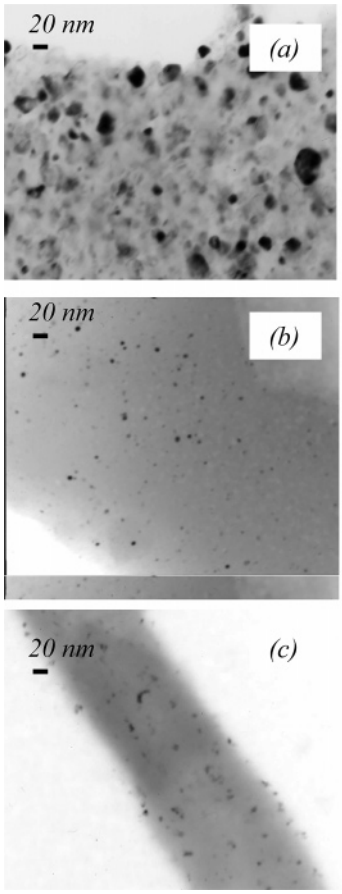

Figure 4. TEM dark-field negative images of the N50 (a), N15 (b), and N5(c) as-prepared samples.

TEM observations show the presence of nanocrystalline particles dispersed in the silica matrix in all the samples. As an example, dark field micrographs of N50, N15, and N5 samples are reported in Figure 4. The amount of visible particles increases with the $CoFe_2O_4$ content; their size increases from an average of about 2 nm (N5) to an average of about 8 nm (N50), and their size distribution becomes larger and larger. The small size and the low number of particles in the diluted samples justify the XRD results. The nanoparticles have spherical shapes in the diluted samples (N15, N10, N5) and more irregular shapes in the ones with higher $CoFe_2O_4$ content (N50, N30).

Figure 5 shows N_2 adsorption/desorption curves at 196 °C. Going from the diluted samples (N5 and N10) to the most concentrated ones, a change of the textural features can be noticed. In fact, N5 and N10 show a type I isotherm with no hysteresis, indicating a totally microporous texture, expected for silica gels prepared under acidic conditions.[34] The N15 sample shows a type I−type IV composite isotherm,

(30) Takahashi, R.; Sato, S.; Sodesawa, T.; Suzuki, M.; Ichikuni, N. *Microporous Mesoporous Mater.* **2003**, *66*, 197.
(31) Yue, Z.; Li, L.; Zhou, J.; Zhang, H.; Gui, Z. *Mater. Sci. Eng., B* **1999**, *64*, 68.
(32) Yue, Z.; Zhou, J.; Wang, X.; Gui, Z.; Li, L. *J. Eur. Ceram. Soc.* **2003**, *23*, 189.
(33) Casu, M.; Lai, A.; Musinu, A.; Piccaluga, G.; Solinas, S.; Bruni, S.; Cariati F.; Beretta, E. *J. Mater. Sci.* **2001**, *36*, 3731.
(34) Brinker, C. J.; Scherer, G. W. *Sol−gel Science*; Academic Press: New York, 1990.

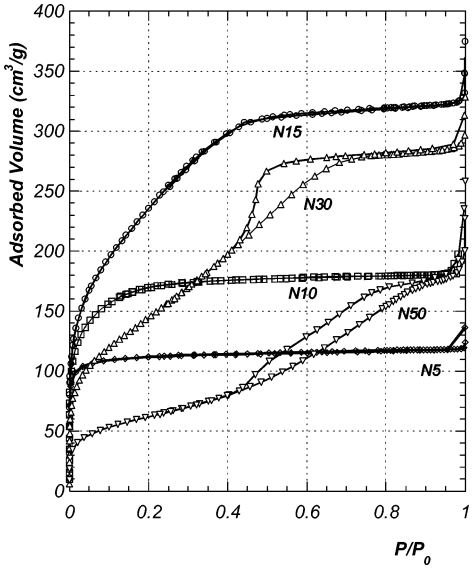

Figure 5. Nitrogen physisorption isotherms recorded at 77K of the as-prepared samples.

Table 2. Textural Properties of the $CoFe_2O_4/SiO_2$ Samples

sample	SA[a] (m^2/g)	av pore size diam (Å)	sample	SA[a] (m^2/ g)	av pore size diam (Å)
N50_as-prepared	221[b]	40	N15_T500	670[c]	6
N30_as-prepared	530[b]	40	N15_T700	678[c]	6
N15_as-prepared	823[c]	6	N15_T900	30[c]	9
N10_as-prepared	676[c]	6			
N5_as-prepared	495[c]	6			

[a] Error 3%. [b] BET surface area. [c] Dubinin surface area.

which could be due either to very narrow mesopores or to a bimodal distribution with one maximum in the micropore and the other in the mesopore range.[35] Finally, the adsorption isotherms of the N30 and N50 samples are of type IV and present hysteresis loops of type H1, indicating that the structure is mainly mesoporous.

The surface area values, reported in Table 2 together with the average pore size, increase from the N50 sample to the N15 sample as a consequence of the increasing porous silica content and then decrease as a consequence of the reduced amount of CA in the diluted gel precursors. These results are in agreement with literature data for silica samples prepared using citric acid.[29] In any case, the surface area values reported for these composites are quite high compared with the results reported in the literature for xerogel samples, while they are comparable to those observed for aerogel samples. This result can be explained by the formation mechanism of the texture; in fact, the self-combustion process induces a swift loss of solvents very similar to solvent extraction in supercritical conditions, thus leading to a preservation of the preexisting gel structure.

The ZFC and FC magnetic susceptibilities were measured but are not reported here. FC and ZFC curves of the diluted samples (N5, N10) coincide, showing a paramagnetic behavior. N15, N30, and N50 samples display a progressively irreversible magnetic behavior (separation of the two curves) due to the increasing presence of superparamagnetic particles;

(35) Vendange, V.; Jones, D. J.; Colomban, P. *J. Phys. Chem. Solids* **1996**, *57*, 196, 1907.

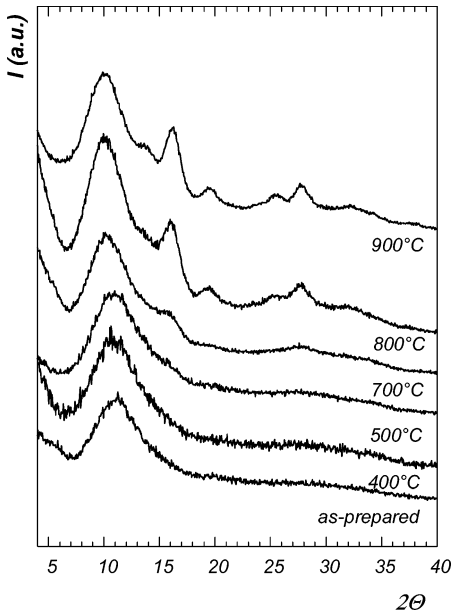

Figure 6. XRD patterns of the N15 sample treated at different calcination temperatures.

this behavior parallels the formation and growth of the $CoFe_2O_4$ nanoparticles in the samples, as evidenced by XRD and TEM results.

Calcined Samples. The progressive heating of the diluted samples leads to the appearance of faint $CoFe_2O_4$ X-ray diffraction peaks, while in the case of the high $CoFe_2O_4$ content samples the peak intensities increase and their broadening slightly decreases.

The XRD patterns of the N15 sample as a function of the thermal treatment are reported in Figure 6. Similar continuous evolution was found for the other two diluted samples. Although the peaks related to the $CoFe_2O_4$ phase can hardly be separated from the amorphous pattern for thermal treatments up to 700 °C, they clearly suggest the presence of small cobalt ferrite particles at 800 and 900 °C. The amorphous background undergoes some modifications as well, indicating structural rearrangement of the silica network. In fact, the silica halo at about $2\theta = 11°$ in the as-prepared sample shifts toward lower angular values ($2\theta = 9.5°$) at 900 °C.

The nitrogen adsorption−desorption isotherms of the samples calcined at different temperatures indicate high surface area values up to 700 °C for all the samples; at higher temperatures a collapse of the structure is observed. As an example, the results obtained for N15 samples at various calcination temperatures are summarized in Table 2. The highest surface area value is observed for the as-prepared sample (823 m^2/g), very high values are obtained also for the samples treated at 500 and 700 °C (670−680 m^2/g), and collapse of the porous structure is observed for the sample heated at 900 °C (30 m^2/g).

The XRD patterns of the samples treated at 900 °C are reported in Figure 7. The peaks of the nanocrystalline phase increase in intensity with $CoFe_2O_4$ content and become sharper and sharper as a consequence of the increase of the particle size.

TEM observations of the samples treated at 900 °C (Figure 8, left side) indicate the crystalline nature of the nanoparticles

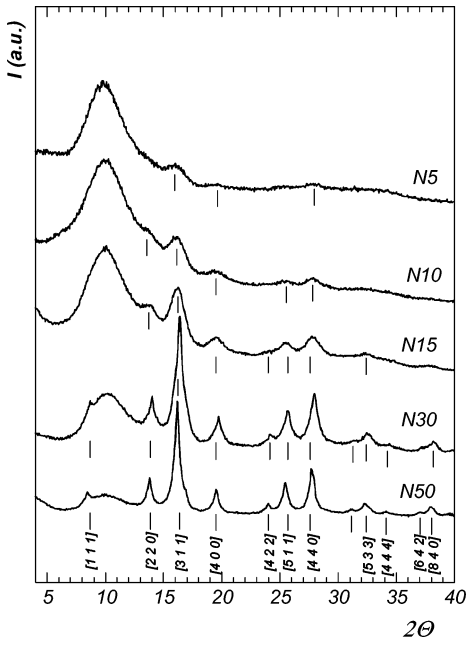

Figure 7. XRD patterns of the samples calcined at 900 °C.

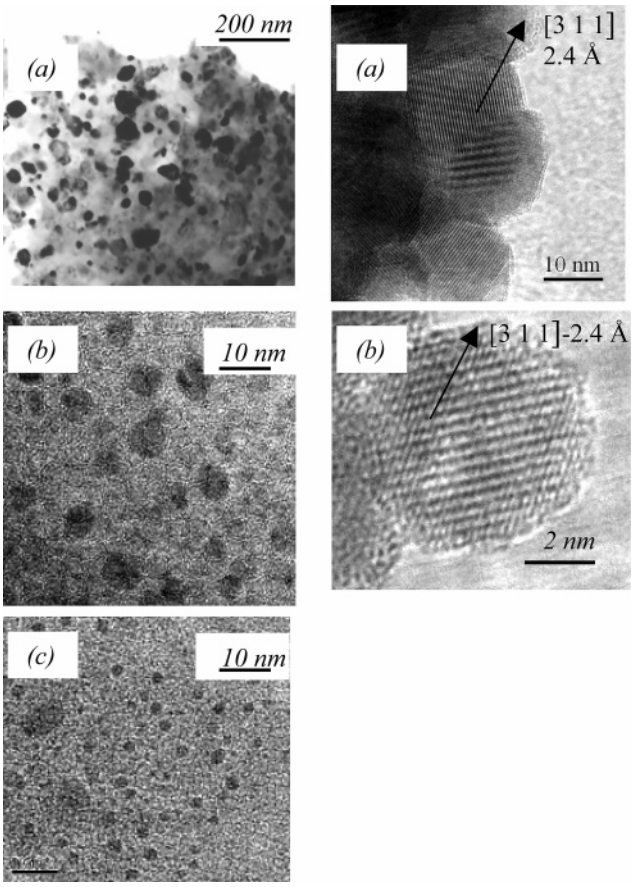

Figure 8. TEM images (left side) of the N50 (a), N15 (b) and N5 (c) samples and HRTEM (right side) images of the N50 (a) and N15 (b) samples calcined at 900 °C.

dispersed in the silica support. The heating process leads to the progressive growth of the particles and to their structural ordering. Therefore, a higher number of particles can be seen in these images in comparison with those of the as-prepared samples. The HRTEM images (Figure 8, right side) confirm the irregular morphology of the particles for the samples with the highest concentration and the spherical morphology of the nanocrystals for the diluted ones. Moreover, a great number of particles are in close contact in the N50_T900 sample, while in the diluted samples the matrix is effective in preventing aggregation. The set of fringes observed in samples N50_T900 and N15_T900 corresponds to the [311] lattice planes of the cobalt ferrite phase with a distance of 2.4 Å.

The particle size distributions are represented with histograms in Figure 9, and the average particle sizes are calculated with a log-normal distribution.[36] The particle size distributions show an increase of the average particle diameter from about 3 nm (N5) to 30 nm (N50), accompanied by a gradual broadening of the particle size distribution.

The magnetic measurements evidence superparamagnetism for all the samples treated at 900 °C, with a hysteretic behavior at low temperature. FC and ZFC curves are reported in Figure 10. In all the samples, the ZFC and FC susceptibilities coincide at high temperature, while in going to low temperatures they start to separate: the FC magnetization increases with decreasing temperature, while the ZFC magnetization shows a broad maximum. The temperature corresponding to the maximum can be related to the blocking temperature, i.e, to the temperature at which the relaxation time is equal to the time scale of the experiment (τ_m). The temperature T_{sep} at which the ZFC and the FC curves separate corresponds to the blocking of the largest particles, while the maximum of the ZFC curve (T_{max}) can be related to the blocking of the particles with average volume.[37,38] The difference $T_{sep} - T_{max}$ is therefore a qualitative measure of the width of the energy barrier distribution and thus of the nanoparticle size distribution. The values of T_{max} and T_{sep} are reported in Table 3. T_{max} increases from 41 K for the N5_T900 sample to 207 K for N50_T900, and $T_{sep} - T_{max}$ shows the same behavior. The observed trend is due to an increase of the average volume and of the width of the particle size distribution, as indicated by TEM observations. However, also interparticle interactions, which are expected to be stronger in samples with higher cobalt ferrite load, can contribute to the observed shift.[39] In fact, the observation that the FC curves of N50 and N30 samples flatten below 25 K suggests the possible formation of a collective magnetic state due to interparticle interactions.[40] For samples N15, N10, and N5 some information about interparticle magnetic interactions can be obtained from the study of the susceptibility in the superparamagnetic region ($T > T_b$). In these conditions the ZFC susceptibility follows, as a first approximation, a Curie−Weiss law:

$$\chi = C/(T - \Theta_{sp}) \qquad (1)$$

where the Curie constant $C = \langle\mu^2\rangle/3k_b\langle V\rangle$ [$\langle\mu\rangle$ is the average

(36) Chantrell, R. W.; Popplewell, J.; Charles, S. W. *Physica* **1977**, *86−88B*, 1421.
(37) Morrish, A. H. *The Physical Principles of Magnetism*; John Wiley and Sons: New York, 1965.
(38) Nèel, L. *Ann. Geophys.* **1949**, *5*, 99.
(39) Dormann, J. L.; Fiorani, D.; Tronc, E. In *Advances in Chemical Physics*; Prigogine, I., Rice, S. A., Eds.; Wiley: New York, 1997; Vol. XCVIII, p 283.
(40) Zysler, R. D.; Fiorani, D.; Testa, A. M. *J. Magn. Magn. Mater.* **2001**, *224*, 5.

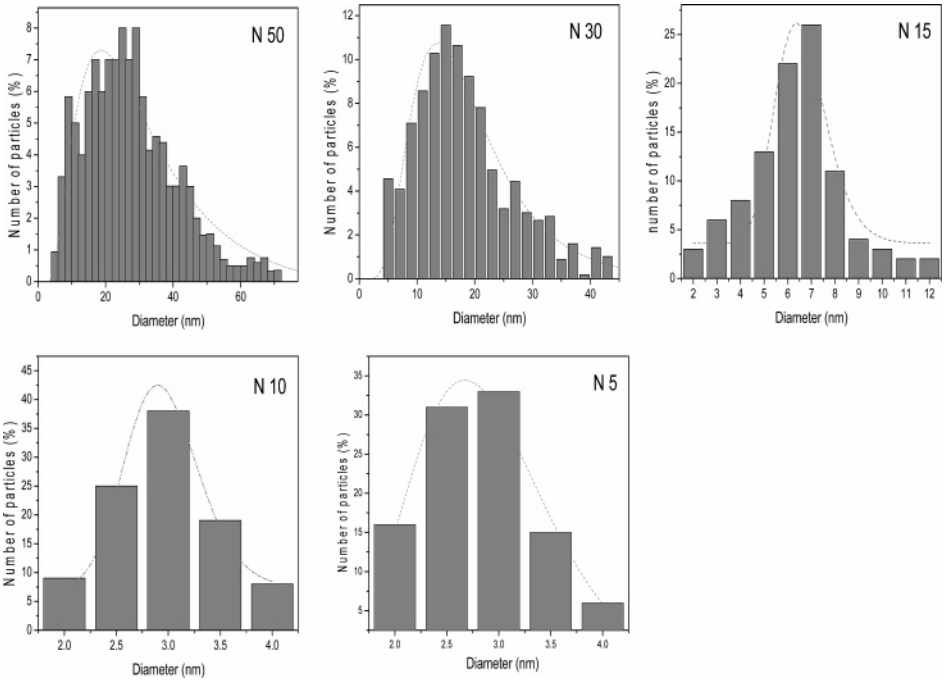

Figure 9. TEM particle size distribution of the samples calcined at 900 °C.

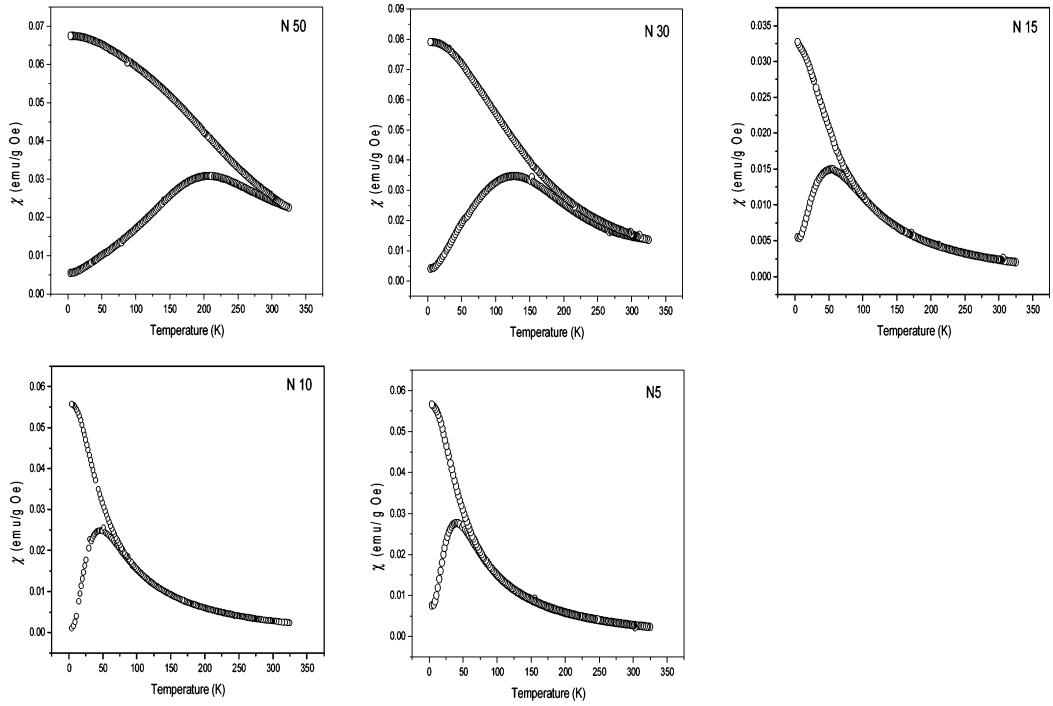

Figure 10. ZFC−FC curves of the samples calcined at 900 °C normalized to the amount of magnetic component.

Table 3. T_{max} and T_{sep} Temperatures Determined from the ZFC−FC Curves[a]

sample	T_{max} (K)	T_{sep} (<3%) (K)	$T_{sep} - T_{max}$ (K)	$\langle D_{TEM} \rangle$ (nm)	rel width σ
N50_T900	207	298	91	28.3	0.6
N30_T900	127	231	104	16.3	0.4
N15_T900	53	85	32	6.6	0.2
N10_T900	49	73	24	2.9	0.1
N5_T900	41	65	24	2.8	0.1

[a] Results of the log-normal fit of the particle size distribution obtained from TEM images.

magnetic moment, k_b the Boltzmann constant, and $\langle V \rangle$ the average nanoparticle volume], T is the absolute temperature, and Θ_{sp} is the superparamagnetic Curie temperature. It must be remarked that this formula is valid for uniaxial nanoparticles, provided that the susceptibility is field independent.[41]

Equation 1 was used to fit the susceptibility for temperatures over T_{sep}, where the ZFC and FC curves coincide and all the nanoparticles are presumably in the superpamagnetic state. Dormann pointed out[42] that Θ_{sp} can provide a rough

(41) Fiorani, D.; Dormann, J. L.; Cherkaoui, R.; Tronc, E.; Lucari, F.; D'Orazio, F.; Spinu, L.; Nogues, M.; Garcia, A.; Testa, A. M. *J. Magn. Magn. Mater*. **1999**, *196−197*, 143.
(42) Dormann, J. L.; Fiorani, D. *J. Magn. Magn. Mater*. **1995**, *140−144*, 415.

evaluation of the strength of the interparticle magnetic interactions. In the N10 and N5 samples the superparamagnetic Curie temperature is close to 0 K, and in the N15 sample the value is at about −7 K. These results suggest that in the most diluted samples (N5, N10) the interparticle interactions are of the same order of magnitude and are unimportant, while in the N15 sample weak magnetic interactions may be present. However, it should be pointed out that the Curie temperature values obtained provide only a first indication of the magnetic interactions, as they do not take into account the dependence of the magnetic moment on the temperature.

Discussion

The preparation route reported here, which combines a traditional sol−gel technique (hydrolysis and condensation of alkoxide precursors) and nitrate−citrate sol−gel self-combustion, has been successful in providing nanoparticles made up of a single $CoFe_2O_4$ spinel phase finely dispersed in a silica amorphous matrix within a wide range of composition (from 5 to 50 wt % cobalt ferrite). In recent years other authors[20,21] have attempted to prepare ferrites dispersed in silica matrixes through a similar sol−gel autocombustion synthesis; XRD, IR, and NMR results have shown difficulties found in the silica polymerization process,[16] hence the problems in obtaining homogeneous composites of ferrite in silica. Through a careful control of several preparation parameters (pH, amount of ethanol, gelation temperature, thermal treatments), the synthesis proposed here has led to a decisive improvement of the nanocomposite properties as regards active phase dispersion, particle shape and size, and particle size distribution.

In all the investigated compositions the thermal analysis has evidenced that the samples form through a self-combustion mechanism. A consequence of this fast combustion process is the high surface area exhibited by all the samples. The silica gel network, filled with amorphous cobalt iron ammonium citrate, does not shrink during the self-propagating combustion process, while condensation of silanols is not inhibited. Thus, a highly open structure is achieved in the whole compositional range explored; it is comparable to that obtained by the more complicated supercritical drying process and is beneficial to the dispersion of the magnetic phase. The final products display combinations of properties typical of the constituent phases, therefore giving rise to new multifunctional materials. For example, the silica open network allows fast diffusion of reactants and products, and the large nanophase dispersion may provide a large number of active sites for catalytic applications.[30,43]

The formation of the carboxylate−metal complexes during the gelation stage, demonstrated by IR measurements, is crucial in the control of the nanoparticle properties. Combining the autocombustion method with appropriate thermal treatments, a wide variety of samples have been prepared in which the magnetic properties are finely modulated.

The ZFC−FC measurements of the samples treated at 900 °C have allowed the study of superparamagnetic relaxation as a function of the $CoFe_2O_4$ load and therefore of the particle size and of the number of particles. In fact, the particle size is strictly related to the magnetic particle blocking phenomenon. T_{max} and T_{sep} increase with increasing $CoFe_2O_4$ content, as expected for increasing average particle size. However, in going from the N15 sample to the more diluted ones, a regular trend cannot be discerned in T_{max} and T_{sep}, the values for N15 being very close to those of N10. This can be ascribed to the fact that the self-combustion process occurs in slightly different ways in the N10 and N5 samples. In the DTA curves the sharp asymmetric exothermic peak, centered at about 200 °C for N15, shifts to 223−230 °C and becomes broader, and its intensity considerably decreases in the case of N10 and N5. This behavior indicates a different speed of the particle formation and growth and might justify the T_{max} and T_{sep} trend. The porosity of N5 and N10 (microporosity) is also different from that of N30 and N50 (mesoporosity), while N15 exhibits intermediate properties.

Besides the size, also the number of particles has a great influence on the magnetic behavior. By increasing the $CoFe_2O_4$ content, the average distance between particles decreases, and therefore, the interparticle interactions increase. The different importance of the interactions can be another reason for the noncompletely regular evolution of the blocking temperatures. In agreement with this, the observed Curie temperature values indicate that the interparticle interactions are unimportant for the N10 and N5 samples while they are weak for the N15 sample.

Interesting results have also been obtained by monitoring the structural and magnetic property evolution of the samples as a function of the thermal treatments. A certain number of particles form through the self-combustion process (as-prepared samples), and then the thermal treatment gives rise to their progressive growth and structural ordering. As a consequence, a greater and greater number of nanoparticles of $CoFe_2O_4$ are observed in TEM micrographs, the $CoFe_2O_4$ reflections become more evident in the XRD patterns, and the morphology becomes more regular together with the particle dispersion and particle size distribution. Obviously, these structural and morphological modifications take place side by side with the evolution of the magnetic properties, which in turn can be modified in a wide range.

In conclusion, the possibility to control the features of the nanoparticles dispersed in the silica matrix makes the sol−gel autocombustion method a very promising route for the deep investigation of the magnetic behavior of nanomaterials.

Acknowledgment. This work was supported by the University of Cagliari and MIUR.

(43) Ramankutty, C. G.; Sugunan, S. *Appl. Catal., A* **2001**, *218*, 39.

CM060650N